Electrokinetic and Optical Detection of Nucleic Acids for Biomedical Diagnosis in Microfluidics

Rui Miguel Raposo Pinto

Thesis to obtain the Master of Science Degree in Biomedical Engineering

Supervisor: Doctor João Pedro Estrela Rodrigues Conde
Co-supervisor: Doctor Francisco Javier Lombardo Enguita

Examination Committee:
Chairperson: Doctor Cláudia Alexandra Martins Lobato da Silva
Supervisor: Doctor João Pedro Estrela Rodrigues Conde
Member of the Committe: Doctor Duarte Miguel de França Teixeira dos Prazeres

June 2014

Abstract

microRNAs are endogenous RNAs with a length of about 22 nucleotides that can play important regulatory roles in the cells. The recent discovery of circulating miRNAs has opened the possibility to study this class of biologically active agents as biomarkers of disease. Lab-on-a-chip systems may play a decisive role in the profiling of microRNAs for point-of-care diagnostic purposes. This thesis explores an electrical, label-free detection principle for microfluidic detection of nucleic acids.

PDMS microchannels were sealed against glass where planar electrodes were previously deposited on. This microfluidic system allowed for electrokinetic and fluorescence measurements. Transient streaming current and potential measurements proved to be accurate in describing the overall electrical surface charge of the channel. For a bare channel, ζ-potential values varied between -67 mV (DI Water) and - 4.6 mV (100 mM PB). In order to recognize the target DNA, the microchannels were functionalized with APTES, ssDNA probe and blocked with BSA. After probe immobilization, the probe density on the surface was 2.09x104 µm-2 (15.7% of a dense monolayer) and, after the blocking step, it dropped to 9.71x103 µm-2 (7.3% of a dense monolayer). Using a 16 nL sample, streaming current measurements allowed to detect 5 µM of target DNA (miR-122 sequence) and distinguish it from a negative control (miR-375 sequence), while the fluorescence measurements detected down to 500 nM target DNA.

A considerable number of enhancements are suggested in order to improve the sensitivity and specificity of the method and to integrate it on a micro total analysis system.

Key Words: *DNA; fluorescence; label-free; microfluidics; microRNA; streaming current*

1. Introduction

1.1. microRNAs as Novel Biomarkers

miRNAs are endogenous RNAs with a length of about 22 nt that can play important regulatory roles in animals and plants by targeting mRNAs for cleavage or translational repression (Bartel, 2004). The importance of miRNA-mediated gene regulation is coming into focus as more miRNAs and their regulatory targets and functions are discovered.

To achieve the goal of early diagnosis and treatment, miRNAs could play an important role. The recent discovery of circulating miRNAs has opened the possibility to study this class of biologically active agents as modes of inter-cellular information flow as well as biomarkers of disease. (Kinet, et al., 2013)

1.2. State of the Art in microRNA Measurement

In general, all miRNA profiling methods can be separated into two categories: one that utilizes direct oligonucleotide hybridization without sample RNA amplification and the other requiring sample amplification. There are inherent advantages and disadvantages to both approaches as protocols that do not perform sample amplification will require a larger starting amount of total RNA, while protocols that require sample amplification could be more prone to handling errors that can also be amplified. (Kong, et al., 2009) Although there is currently no gold standard, there are some mainstream methods to detect and measure the expression levels of miRNAs, all of which face unique challenges: northern blotting (NB), microarray hybridization, quantitative real-time reverse-transcription polymerase chain reaction (qRT-PCR), and next-generation sequencing (NGS). (Git, et al., 2010) (Koshiol, et al., 2010)

Microarray technology was developed in 1995, allowing multiple hybridizations to occur in parallel, on a glass or quartz support where antisense probes are immobilized. (Liu, et al., 2008) Direct hybridization of samples onto an oligo array may require a large amount of miRNA, but some samples provide only a small and limited amount of RNA. (Kong, et al., 2009) Polymerase chain reaction (PCR)-based approaches have been developed to address this issue. (Schmittgen, et al., 2004) The major advantages of qRT-PCR over microarrays are the sensitivity of the qPCR assays, a considerably larger dynamic range compared to microarray analysis and a convenient requirement for low amounts of starting material (in the range of nanograms of total RNA). (Benes

& Castoldi, 2010) However, the analysis of the expression of known miRNAs using qRT-PCR is both time and reagent consuming. Recently, different approaches to perform parallel reverse transcription for a large number of miRNAs contained in a single sample have been reported, bringing the possibility of high-throughput analysis. (Tang, et al., 2006) (Moltzahn, et al., 2011) (Chen, et al., 2009)

Platforms such as microarray and qRT-PCR can only identify known sequences, which makes them good miRNA profiling tools but with little utility for miRNA discovery. NGS allows both discovery of new miRNAs and confirmation of known miRNAs in a high-speed, high-throughput fashion without the need for gels or the ambiguity in data interpretation inherited by other methods. (Koshiol, et al., 2010)

It is considered good practice to profile miRNAs by microarray followed by validation with qRT-PCR. (Koshiol, et al., 2010) However, there are no standard guidelines for conducting and reporting such validation. For example, some authors report validation by qRT-PCR for some miRNAs and by Northern blot for other miRNAs, or report validation of precursor but not mature miRNAs. (Koshiol, et al., 2010) Furthermore, there is no standard as to which internal control should be used for the normalization of qRT-PCR, which can result in erroneous conclusions. Standardized guidelines would aid the interpretation of miRNA data by creating transparency in reporting.

1.3. Microfluidics and Lab-on-a-Chip (LOC)

The study of fluid motion in microsystems is denoted as microfluidics. (Bruus, 2008) There are several advantages of scaling down standard laboratory setups by a factor of 1000 or more, from the decimeter scale to the 100 µm scale. One obvious advantage is the dramatic reduction in the amount of required sample. A LOC system can easily deal with as little as 1 nL or 1 pL. Such small volumes allow for very fast analysis, efficient detection schemes, and analysis even when large amounts of sample are unavailable. To handle small volumes, it is possible to develop compact and portable systems that might ease the use of bio/chemical handling and analysis systems tremendously.

Some of the efforts towards miRNA profiling in microfluidics consist on the miniaturization and automation of conventional laboratory techniques (e.g. qRT-PCR), with low novelty regarding detection schemes. Other approaches take advantage of the microfluidic scale phenomena (e.g. laminar flow), leading to the development of original ideas for the detection of biomolecules in microfluidic systems.

Electrokinetic phenomena can play important roles in microfluidics, as they can be applied to fluid pumping, separation processes and detection. In a work developed at INESC-MS's facilities, label-free electrical detection of surface DNA immobilization and hybridization via streaming current measurements were demonstrated. (Martins, et al., 2011) Streaming currents generated by the flow of deionised water through a PDMS microchannel sealed on glass were measured using integrated Au electrodes. This technique was sensitive to the density and polarity of the charge on the channel surface, allowing the recognition of DNA hybridization and distinguishing between assays with complementary and non-complementary DNA strands. Later, more experiments with integrated miniaturized electrodes were performed. (Martins, et al., 2013) Experiments using solutions with different salt concentrations and different electrode materials showed that the measured electrical current depends on the electrode material and in general differs from the real value of the streaming current. An equivalent circuit model was proposed, as well as potential sources of error that can affect the streaming current measurements and suggestions on how to correct the measured values. These works on streaming currents in microfluidics, measured with integrated, planar, polarizable electrodes constitute the foundation of this work.

2. Streaming Current in Microfluidics

The substrates employed in the current work are glass and PDMS. Glass acquires a negative charge when in contact with water mainly due to the dissociation of silanol groups (Grier, 2001):

$$SiOH \Leftrightarrow SiO^- + H^+ \quad (1)$$

Additionally, after the treatment used to seal the glass against the PDMS surface, the inner surface of the channel will be negatively charged by hydroxyl groups at the surface.

The solution in contact with the channel is electrically neutral, having an equal number of cations and anions. However, due to the surface charge at the solid phase, a number of oppositely charged ions (counterions) will be attracted to the region near the surface (electrostatic attraction) and the ions of the same charge (coions) will be repelled away from the surface, which results in a positive net charge in this region. The concentration of counterions decreases with the distance from the surface while the coion concentration increases with the distance from the surface. In the bulk of the solution, far from the surface, the counterion and coion concentrations are the same and the resulting charge is zero. In the case of glass, because the surface acquires negative charge, the counterions are positively charged. The surface charge in the solid phase is balanced by the counterions in the liquid phase. Electric double layer (EDL) is the name usually given to the charged surface of the solid plus the balancing counterion layers in the liquid.

The counterions closer to the surface charges will be strongly attracted to the surface, forming a layer (compact layer) that is immobile. As the distance from the surface increases, the electrostatic attraction is weaker, making these counterions mobile (diffuse layer). The boundary between the compact and the diffuse layer is usually referred to as the shear plane. Usually, the liquid velocity is considered to be zero at this plane. The surface potential is difficult to measure, but the potential at the shear plane,

which is called the zeta (ζ) potential, is often considered as an approximation to the surface potential.

Since the diffuse layer (Debye layer) has a net charge density, if a flux is established inside the microchannel, it will drag the mobile counterions, generating a net current known as streaming current. The streaming current is usually measured by an ammeter with very low internal resistance connected to two electrodes, one at the inlet and the other at the outlet of the microchannel. The current induced by the flow is given by:

$$I_S = \int_A \rho \, \vec{u} \, dA \tag{2}$$

where the integral is taken over A, the cross-sectional area of the microchannel. $\vec{u}$ is the flow profile and ρ is the charge density at the surface. In general, one must solve the Poisson-Boltzmann equation to get ρ and the Stokes equations to get $\vec{u}$, for each individual geometry. In the limit of Debye-Hückel linearization and Debye layers that are thin compared to channel diameter or height, a simplified approximation is possible. (Kirby & Hasselbrink, 2004) As long as the flow is laminar, the streaming current (I_S) dependency on the pressure drop (ΔP) is given by:

$$I_S = \frac{\varepsilon_0 \, \varepsilon_r \, A}{\mu \, L} \, \zeta \, \Delta P \tag{3}$$

where A is the channel cross-section, L is the length of the channel, μ is the dynamic viscosity of the solution, ε_0 is the vacuum permittivity, ε_r is the relative permittivity of the solution and ζ is the zeta-potential characteristic of the solution and solid in contact.

If, instead of closing the external circuit through an ammeter, one connects the electrodes to a voltmeter (with very high internal resistance), the counterions will accumulate at the outlet of the microchannel, developing a difference of potential (streaming potential) between the extremes of the channel. The streaming potential ($\Delta\phi$) is related to the pressure drop (ΔP) by the Smoluchowski equation (Kirby & Hasselbrink, 2004):

$$\Delta\phi = \frac{\varepsilon_0 \, \varepsilon_r}{\mu \, \sigma} \, \zeta \, \Delta P \tag{4}$$

where σ is the channel conductivity. In a rectangular cross-section microchannel, for a steady, fully developed laminar flow, the pressure drop (ΔP) and the flow (Q) are related via (Sze, et al., 2003):

$$\Delta P = \frac{12 \, \mu \, L}{h^3 \, w} \, Q \tag{5}$$

where L, h and w are, respectively, the length, height and width of the channel. Replacing ΔP by Q in (3) and (4), using (5), the streaming current and potential in function of the flux (Q) are given, respectively, by:

$$I_S = \frac{12 \, \varepsilon_0 \, \varepsilon_r}{h^2} \, \zeta \, Q \tag{6}$$

and

$$\Delta\phi = \frac{12 \, \varepsilon_0 \, \varepsilon_r \, L}{\sigma \, h^3 \, w} \, \zeta \, Q \tag{7}$$

According to (6) and (7), the zeta-potential can be calculated from the slope of the streaming current vs flux or the streaming potential vs flux representations.

In a streaming current experiment, the counterions are constantly being pumped into the inlet and depleted in the outlet (Figure 1). The streaming current flows with the liquid, along the channel, while two other phenomena neutralize it. (Martins, et al., 2013) The first is the faradic current that flows through the electrodes and low impedance external circuit, originated by electrochemical reactions at the electrode surfaces. The second is an ionic conduction current which flows along the microchannel, in the opposite direction of the streaming current, due to the induced electric field in solution acting on the ions inside the microchannel. For charge conservation, the streaming current must be equal to the sum of these two currents.

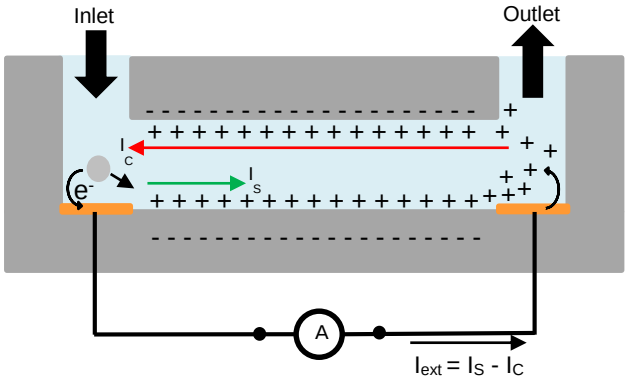

Figure 1 – Schematic of the streaming current (I_S), conduction current (I_C) and external (faradic) current (I_{ext}), established during a streaming current experiment inside a microchannel. For charge conservation, $I_S = I_C + I_{ext}$.

The value of the faradic current, measured by the ammeter, is proportional to the exchange current density, which reflects the intrinsic rates of electron transfer between the analyte and the electrode. This parameter depends on the material properties of the electrode and on the nature of the electroactive species in solution. On the other hand, the conduction current magnitude is inversely proportional to the electrical resistance of the electrolyte inside the microchannel.

The electrode characteristics, in particular its polarizability, have an impact on the accurate streaming current measurement. This implies that the current values recorded with an ammeter have to be adequately treated in order to yield the real streaming current values.

3. Experimental Methods

3.1. Solution Preparation

A 1.0 M potassium chloride (KCl) stock solution was prepared by dissolving the salt crystals (Sigma-Aldrich 60130) in DI water. To perform mass measurements, a

Scientech SA 80 analytical scale was used. All other KCl solution were prepared by sequential dilution from the stock solution. All PB solutions were prepared from a 1.0 M PB stock (Sigma-Aldrich P3619 potassium phosphate buffer, pH=7.4 at 25 ºC), by sequential dilution, using DI water. Phosphate buffered saline (PBS) was prepared by dissolving one tablet (Sigma-Aldrich P4417) in 200 mL of DI water, yielding 0.01 M phosphate buffer, 0.0027 M potassium chloride and 0.137 M sodium chloride, pH=7.4, at 25 °C.

In order to silanize the surface, a 2% (v/v) solution of (3-Aminopropyl)triethoxysilane (APTES) in acetone was prepared from a 99% APTES stock solution (Acros Organics 430941000).

Two surface blocking agents were tested in this work, namely bovine serum albumin (BSA) and salmon sperm DNA. The 2% (w/w) BSA solution in PBS was prepared from a Sigma-Aldrich A7906 stock. The salmon sperm DNA working solution, with 100 µg/ml concentration, was prepared by dilution of the 10 mg/ml stock (Stratagene Sonicated Salmon Sperm DNA, CAT#201190-81) in 100 mM PB.

3.2. DNA Oligonucleotides

Synthetic DNA oligonucleotides (synthesized by STAB VIDA Genomics LAB, Caparica) were used as probe, complementary target and non-complementary target (negative control). The probe oligonucleotides were labelled with 6-FAM, while the target oligonucleotides were labelled with DY560. These fluorophores have distinct excitation and emission bands, and upon the use of proper microscope filters, the probe and target oligonucleotides were imaged separately.

For the experiments to be more realistic with respect to the biomedical application, the complementary target sequence corresponds to the mature sequence of miR-122 (hsa-miR-122-5p according to miRBase.org, release 20), a miRNA that has is upregulated in cases of liver injury and also in heart failure. The probe is the reverse complementary (antiparallel) sequence of miR-122. For negative control (non-complementary target), the sequence of miR-375 (hsa-miR-375 according to miRBase.org, release 20) was used.

The DNA working solutions, with different final concentrations, were prepared with PB, by sequential dilution from the stock, aliquoted and stored at -20 ºC prior to use.

3.3. Surface Functionalization Protocol

The surface functionalization provides the microchannel with biorecognition capabilities.

An unused channel was washed with DI water at 5µl/min for 15 minutes and then a 2% (v/v) solution of APTES in acetone was injected in the channel and incubated for 2 hours, without flow. The APTES reacts with the hydroxyl groups on the surface, forming siloxane covalent bonds. The channel was then washed with acetone for 10 minutes and DI water for 15 minutes, both steps at 10 µl/min.

The ssDNA probe was electrostatically immobilized by injecting a 5 µM solution of ssDNA probe in the channel and incubating it for 1 h 30 min without flow. The channel was then flushed with 100 mM PB for 10 minutes at 5 µL/min to remove non-immobilized ssDNA probe.

Supposing that the APTES and the probe may not cover the surface completely, a surface blocking agent should be used (BSA, for example). A 2% BSA solution in PBS was inserted in the channel and incubated for 1 h. Afterwards, the channel was washed with PBS for 10 minutes at 5 µL/min to remove BSA not bound to the surface.

Finally, the solution containing the ssDNA target (either complementary or non-complementary) was inserted in the channel and incubated for 1 h 30 min without flow, followed by washing with 100 mM PB for 5 minutes at 5 µL/min to remove non-hybridized target.

Usually, both the streaming current and the fluorescence were measured after each of the previously described steps.

3.4. Microfluidic Device Fabrication

The microchannels (length=4 mm, width=200 µm, height =20µm) were patterned on PDMS using a SU-8 mould. Inlet and outlet holes were manually punched. The microchannels were sealed against glass where TiW planar electrodes were previously deposited on. This microfluidic system allowed for electrokinetic and fluorescence measurements.

The bonding was achieved by first exposing the PDMS and glass surfaces to a UV/Ozone treatment, for 6 minutes, on a UVO Cleaner (Model 144AX-220 by Jelight Company). After the UVO treatment, the microchannels and the electrodes were manually aligned on a low power AMSCOPE microscope. The chip was pressed by hand with uniform pressure and was heated at 70 ºC for 30 minutes in a Memmert oven to complete the bonding.

Having the devices sealed, there was the issue of interconnecting the microfluidic chip with the pumping system (New Era NE-300 syringe pump) and with the picoammeter (Keithley 237 source-measure unit) in order to perform the experiments. The fluidic connection was performed by inserting stainless steel adaptors in the inlet and outlet of the microchannel and by connecting those adaptors to 1ml luer-lock syringes using PTFE tubing. A homemade PMMA chip holder was prepared in order to make electrical connections to the TiW pads on the chip.

3.5. Streaming Current and Fluorescence Measurements

The streaming current was measured using a Keithley 237 picoammeter. The determination of the real streaming current value from the measured external current was studied by (Martins, et al., 2013). If the flowing solutions have low ionic concentrations (up to 10^{-4}M), the measured current does not have a transient behavior and it corresponds to the real streaming current inside the channel. For higher counterion concentrations,

the channel resistance decreases, and that, together with the polarizability of the electrodes, results in a transient behavior of the measured current. In the case of transient behavior, the current peak, right after initiating the flow, corresponds to the real streaming current value.

The streaming current was measured after each protocol step. Afterwards, the microfluidic chip was took to the fluorescence microscope for imaging. A Leica DMLM microscope, equipped with a 20X objective (20X/0.4, N PLAN, Leica Germany, 566026), was used for the fluorescence imaging. The images were acquired with a Leica DFC300FX camera. The exposure used was 2.0 s, gain=1 and gamma=1. Leica I3 filter was used to image the probe molecules (6-FAM labelled) and the TX2 filter was used to image the target molecules (DY560 labelled).

The measurements were performed at ambient temperature, kept controlled by the air conditioning system, between 22 ºC and 24 ºC.

3.6. DNA Surface Density Calibration Using the Nanoplotter

At a certain point of the work, it was important to calculate the density of DNA molecules at the surface of the microchannels using fluorescence intensity.

To perform this calibration, micro spots of oligonucleotide solutions were dispensed on the surface of PDMS. If the DNA concentration and volume of such spots is well known, then it is possible to calculate the number of molecules in each spot. After imaging, the area of the spot was calculated and it was possible to make a correlation between the molecule density (number of molecules/surface unit) and the mean fluorescence intensity of the spot.

The SIM Nanoplotter 2.1, equipped with a NanoTip (piezoelectric tip), it able dispense volumes as low as 56 pL in predetermined positions of the PDMS microchannel. Given the dimensions of the microchannel, a volume of 1.12 nL, corresponding to 20x56 pL droplets, proved to be an adequate volume. The PDMS chips (not sealed) were treated with UVO and silanized (2% APTES in acetone, for 2 h). The oligonucleotide solutions were prepared in 10 mM PB, and contained 5% glycerol so that the drops dried slowly. Relative humidity during spotting was 70% to allow slow drying of the spotted solutions.

4. Results and Discussion

4.1. Measurements with DI Water, KCl and Buffer Solutions

After fabricating the first microfluidic devices, the former step was to measure the streaming current while running DI water, KCl solutions and buffer solutions (PB and PBS), in order to verify that the streaming current values were accurate. By varying the flow rate, it was possible to verify the linear relationship between the streaming current and the flow rate, which was expected (see Expression 6).

When the streaming current values are positive, the counterions are positive and the glass/PDMS surface charge is negative. This was expected given that the running solutions had pH ranging from 5.7 (DI water in equilibrium with the atmosphere) to 7.4 (PB and PBS buffers) and the isoelectric point (pI) of glass is pI = 2.1. (Lameiras, et al., 2008)

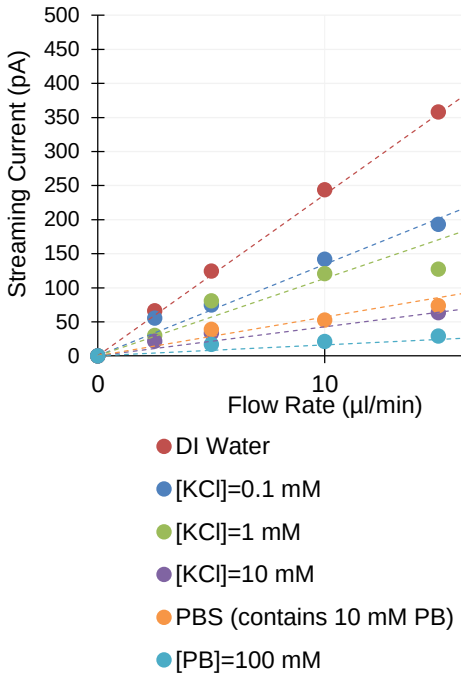

Figure 2 – Linear dependency of the streaming current on the flow rate, for DI water, KCl solutions, PB and PBS.

The streaming current values are higher for more dilute solutions, and hence the slopes of the current vs flow plots are higher for the lower counterion concentrations. According to expression (6), the slope of the current vs flow rate plot depends directly on the ζ-potential. This means that different ζ-potentials can be calculated from the slopes of the graphical representations above. Also obvious at this point is the fact that the ζ-potential depends on the counterion concentration.

If the surface charge density is unaffected by counterion strength, and all the shielding is performed by the diffuse portion of the double layer, then the dependence of ζ on counterion concentration (given constant temperature and dielectric constant) can be shown to be (Kirby & Hasselbrink, 2004):

$$\zeta \sim \lambda_D \sim a_0 + a_1 \log c \qquad (8)$$

where λ_D is the Debye length (characteristic thickness of the EDL), a_0 and a_1 are constants and c is the counterion concentration, for a symmetric electrolyte with counterions of valency equal to 1. In the case of KCl or KH_2PO_4 (contained in PB and PBS), the counterion is K^+ and expression (8) should apply. The previous expression applies for relatively low counterion concentrations and high ζ-potentials (generally applicable for silica below 100 mM at pH=6 and below 10 mM at pH=3.5). (Kirby & Hasselbrink, 2004)

The results for KCl at 10 mM are very similar to the ones for PBS. PBS consists of 10 mM phosphate buffer (KH_2PO_4), 2.7 mM KCl and 137 mM NaCl. Despite the 137 mM of NaCl in the PBS, which contribute with Na^+ counterions, it seems that the K^+ counterions are more relevant to the streaming current measurements. This may be due to the different solubility (ion hydration) of Na^+ and K^+ counterions. Na^+ has a higher solubility than K^+ in water (Baldwin, 1996), meaning that it is more hydrated by the water molecules. Na^+ will be less attracted to the glass surface because its charge is more shielded by the water molecules than K^+. It now makes sense that K^+ counterions, more attracted to the interface, have more influence in the streaming current measurements than Na^+ counterions. The same rational would apply for any other ionic species with different solubilities. Other factors that modify the ζ-potential, and hence, the streaming current, are the pH and the temperature. (Kirby & Hasselbrink, 2004)

At this stage, measurements of the streaming potential were attempted, in order to verify if there was any advantage in using the streaming potential instead of the streaming current. According to expression (7), the streaming potential should also have a linear dependency on the flow rate, which was verified for the various solutions (different counterion concentrations). The streaming potential behavior in time is identical to the streaming current behavior, and may be constant or transient in time, depending on the flowing solution. However, the Keithey 237 instrument used to perform the measurements has a better current sensitivity, and, therefore, there was apparently no advantage in using the streaming potential instead of the streaming current.

Given that both streaming current and streaming potential measurements were available, the ζ-potentials were calculated from both sets of data, for comparison. However, in order to use equation (7) for the ζ calculations from the streaming potential data, the apparent conductivities of the channels needed to be measured. This was made in an approximate manner, without flow in the channel, for the various solutions. The flow may modify the channel conductivity, but this was ignored. An I-V curve was acquired with the channels filled with each one of the solutions, the electrical resistance of the channel was obtained from the slope of such I-V curves and the conductivities (S/m) were calculated using:

$$\sigma = \frac{1}{\rho} = \frac{R\,l}{A} \qquad (9)$$

where ρ (Ω.m) is the electrical resistivity, R (Ω) is the electrical resistance, A (m^2) is the cross-sectional area of the microchannel ($4x10^{-9}$ m^2) and l is the length of the microchannel ($4x10^{-3}$ m).

The conductivity is proportional to the current that flows between the electrodes. For current to flow, ions must be present in solution to carry the charge from one electrode to another. Increasing the number of ions in solution will increase the amount of charge that can be carried between electrodes and will increase the conductivity. This is why solutions with higher ionic strength decrease the channel resistance and increase the conduction current that tends to neutralize the streaming current, making the readings transient in time and more difficult to perform.

The electric conductivity through the bulk of the solution can be considered as the sum of the contributions due to the various ionic species in solution:

$$\sigma = \sum_i |z_i|\, u_i\, C_i \qquad (10)$$

where z_i is the charge (valency) of each ionic species, C_i is the concentration of the species and u_i is the limiting velocity of the ion in an electric field (index of migration velocity). (Bard & Faulkner, 2001)

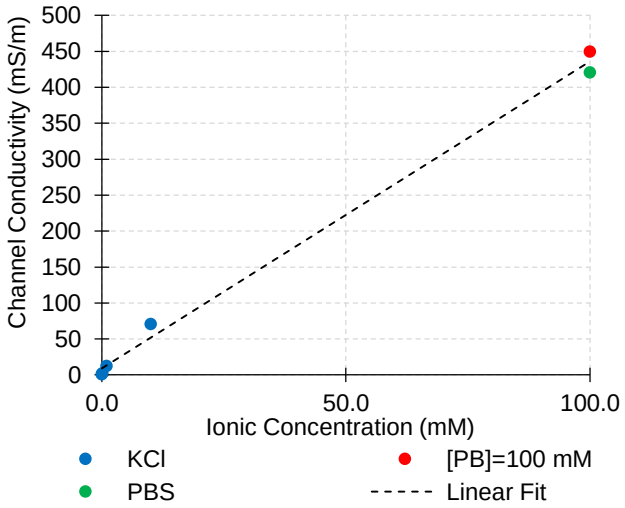

Figure 3 – Apparent conductivity of KCl, PB and PBS solutions in the microchannel, in function of the ionic concentration.

The channel conductivity is apparently linear on the ionic concentration of the solution. Looking at expression (10), if we consider that the z=1 and the index of migration velocity index (u) is identical for all the ionic species in solution, then the conductivity will depend linearly on the total concentration of ionic species in solution. Looking at Figure 3, an interesting fact is that a PB solution at 100 mM has an identical conductivity to PBS (137 mM NaCl, 10 mM PB), given that the total ionic concentration for PB and PBS is identical. This corroborates the theory that the conductivity depends linearly on the ionic strength of the electrolyte, and can be approximated by (10).

After obtaining the conductivities, the ζ-potentials could finally be calculated from both sets of data (streaming current and streaming potential), using expressions (6) and (7). The electric permittivity of vacuum was considered to be ε_0 = 8.854187817x10^{-12} F m^{-1} (Mohr, et al., 2012) and the relative permittivity of the solutions were considered constant and equal to the relative electrical permittivity of water at 24 ºC, ε_r = 78.5 (Fernández, et al., 1995).

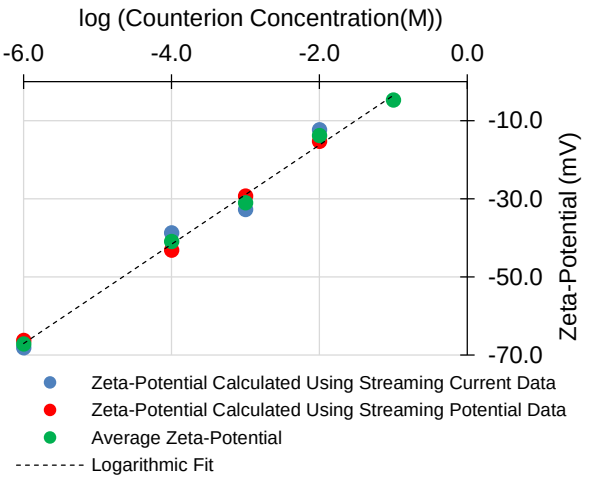

Figure 4 – Zeta potential in function of the total ionic concentration of the solutions flowing in the microchannel.

As can be observed, there is a logatithmic dependency of the ζ-potential on the ionic strength of the solution. This behavior was expected and was discussed above (see expression (8)). A logarithmic regression yielded the following experimental dependency of the ζ-potential on the total ionic concentration of the solution (C) :

$$\zeta = 12.69 \log(C) + 9.1389 \qquad (15)$$

where ζ is in units of mV and C is in units of molar (mol/L).

The results are identical when calculating the ζ-potential using the streaming current data and the streaming potential data, meaning that the measurements are robust. This also means that the approximations made in the calculations were reasonable (the conductivity measurements were performed with no flow, the electrical permittivity of the solutions was considered to be constant, the thickness of the EDL was considered to be much smaller than the other channel dimensions, among other approximations). Finally, the ζ-potential values were comparable to the literature. (Kirby & Hasselbrink, 2004)

4.2. Detection of 5 µM Target DNA

The complete functionalization protocol was performed, followed by the ssDNA target incubation and by a series of stringent washings. The streaming current and the fluorescence were measured at each step.

As expected, the APTES reacts with the hydroxyl groups on the surface, forming siloxane covalent bonds with the glass. The amine groups of the APTES (pKa of about 10) are protonated when in contact with water. (Gubala, et al., 2013) Therefore, the surface is predominantly positive at pH~7, inverting the streaming current sign. At this moment, most of the surface charge is positive and, thus, the counterions are negative in nature.

After incubating the ssDNA probe, the streaming current amplitude decreased slightly (a difference of 0.19 units, which corresponds to a 19% change relative to the absolute amplitude of the initial streaming current), indicating that probably only a relatively small amount of the surface was covered by the probe. Considering that all the DNA backbone phosphate groups contribute ($pK_a<1$) with a negative charge, then a simplistic value for the surface coverage by the probe is 19%, right after the immobilization. The probe fluorescence (6-FAM labelled), measured with the I3 microscope filter, increases dramatically after the probe immobilization.

After the surface blocking with BSA, the streaming current was not significantly modified. However, the probe fluorescence decreased to about half, meaning that a significant fraction of the probe was lost after the blocking step, probably due to competition for the surface or due to the washing with PBS after the blocking step. PBS possesses a significant ionic strength (137 mM NaCl and 10mM PB), meaning that the ions in solution may shield the APTES and the ssDNA probe charges, reducing the intensity of the electrostatic interaction and making the probe more prone to desorption from the APTES surface. Given that the fluorescence drops about 46% after the blocking, and considering the previous estimate of 19% coverage right after the probe immobilization, a rough estimate for the surface coverage after the surface blocking is of about 9%. If there is less probe on the surface but the streaming current is identical, this means that BSA also contributes with a negative charge. The isoelectric point of BSA is pI=4.7. (Ge, et al., 1998) For DI water, at pH~6, BSA is slightly negatively charged. This, together with the fact that BSA may shield the APTES on some locations (the amine groups will not be so exposed and will not contribute with positive charge), explains why the streaming current reading didn't change considerably after the blocking step.

After the target hybridization, the streaming current values measured with 100 mM PB are very small in amplitude (as previously discussed, higher ionic strength solutions lead to the decrease of the zeta-potential and the streaming current) and cannot be used to distinguish between complementary and non-complementary targets. However, the target (DY560-labelled) fluorescence measurements, performed with the TX2 filter, are clear in distinguishing both targets, with a ratio of complementary/non-complementary equal to 2.6. The probe fluorescence on the complementary and non-complementary channels are similar.

After a more stringent wash, with 10 mM PB, the ratio of complementary/non-complementary signal in terms of fluorescence increases to 6. The decrease in the ionic strength of the solution contributed to an increase in the specificity of the essay, given that the control target, with low complementarity to the probe, got more loosely bound and more prone to wash. The amplitude of the streaming currents increased significantly and at this point the best complementary/non-complementary signal ratio, of about 1.9, was obtained. Looking at the error bars, one concludes that the streaming current measurements are less reproducible than the fluorescence measurements. Temperature may play an important role

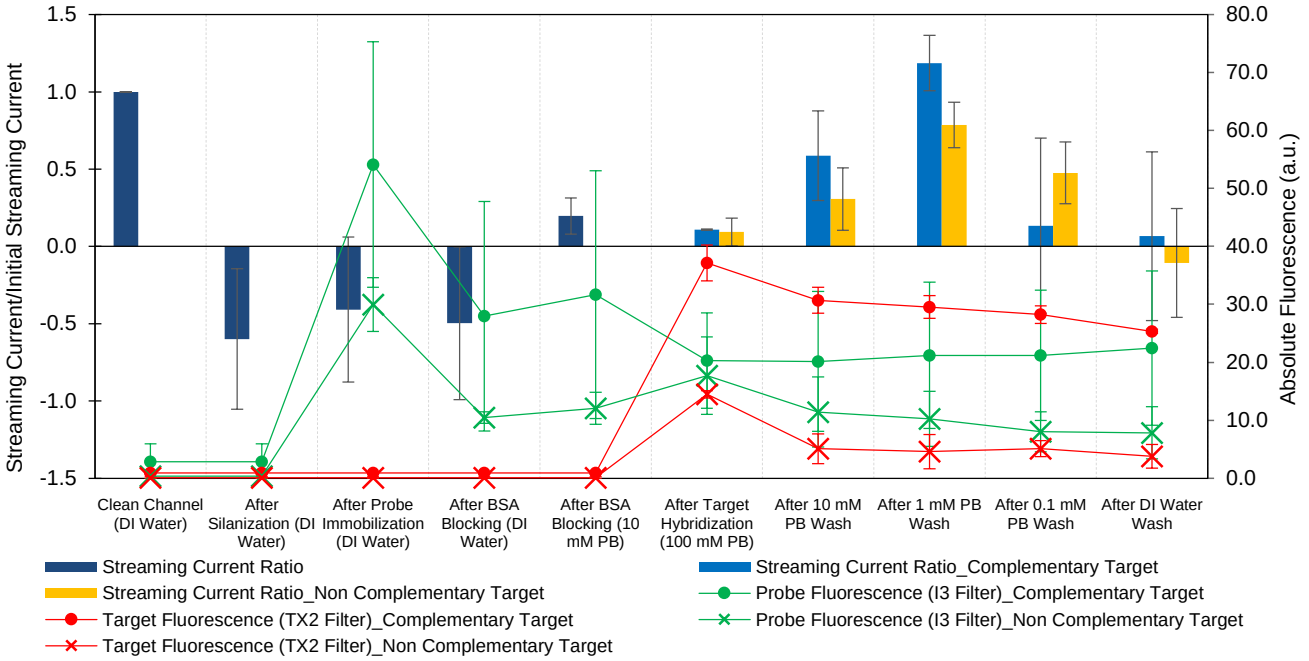

Figure 5 – Streaming current and fluorescence measurements after each functionalization step, culminating in the detection of 5 µM of target DNA. It is possible to distinguish between a fully complementary DNA target (miR-122) and a DNA control target (miR-375). The error bars represent the standard deviation due to inter-experimental and device batch variations.

in all the steps of the experiment, and, as was previously discussed for the zeta-potential, temperature changes lead to variations in the streaming current measurements.

From this experiment, it was concluded that the optimal PB concentration to perform both the streaming current and the fluorescence measurements is 10 mM. It was also noticed that, with the present surface functionalization protocol, the streaming current is at the limit of its capabilities in distinguishing between the fully complementary and the non-complementary targets.

4.3. Towards the Detection of Lower Target Concentrations

After the successful detection of 5 µM, an experiment with lower DNA target concentration (500 nM) was performed in order to assess the sensitivity of the system. The streaming current measurements did not distinguish between a fully complementary DNA target (miR-122) and a non-complementary DNA control target (miR-375), but fluorescence did.

Working towards the detection of lower target DNA concentrations using the streaming current, the surface blocking step was optimized by testing different blocking agents. Also, because the target capture reaction may be limited due to target molecule depletion near the surface, flow target incubation instead of static incubation was attempted.

4.3.1. Blocking Step Optimization

Non-specific adsorption of the non-complementary target molecules directly on the positively charged APTES surface may decrease the specificity of the detection scheme. Salmon sperm DNA was tested as blocking agent and compared to BSA and a control (no blocking after the probe immobilization).

Looking at the comparison of the three experiments, the blocking agent that leads to the best complementary/non-complementary signal ratio, both in terms of the streaming current and the fluorescence, is BSA. Given this conclusion, BSA continued to be used as blocking agent in the following experiments.

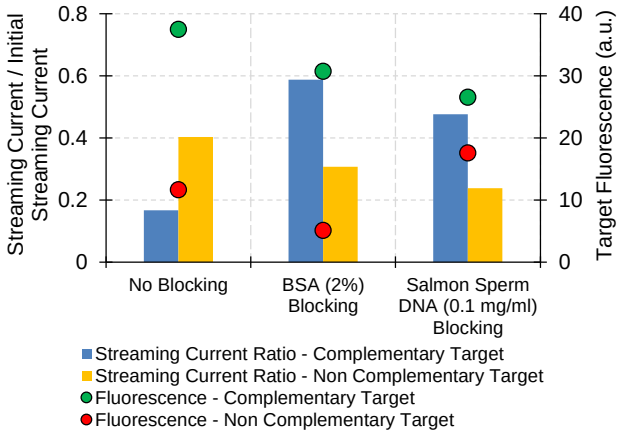

Figure 6 – BSA and salmon sperm DNA as surface blocking agents, compared to a control (no blocking). Streaming current and target fluorescence (TX2 filter) after the 10 mM PB wash step.

4.3.2. Steady State vs Flow Incubation

To avoid limiting the target capture reaction by molecule depletion near the surface (due to steady state incubation), several experiments with target incubation in

flow conditions were performed. The protocol was the same as before, except for the target incubation step that was performed at a flow rate of 0.5 µl/min for 10 min. Experiments were performed for 5 µM and 500 nM target concentrations, and the results after hybridization plotted with the previous incubation results (Figure 7).

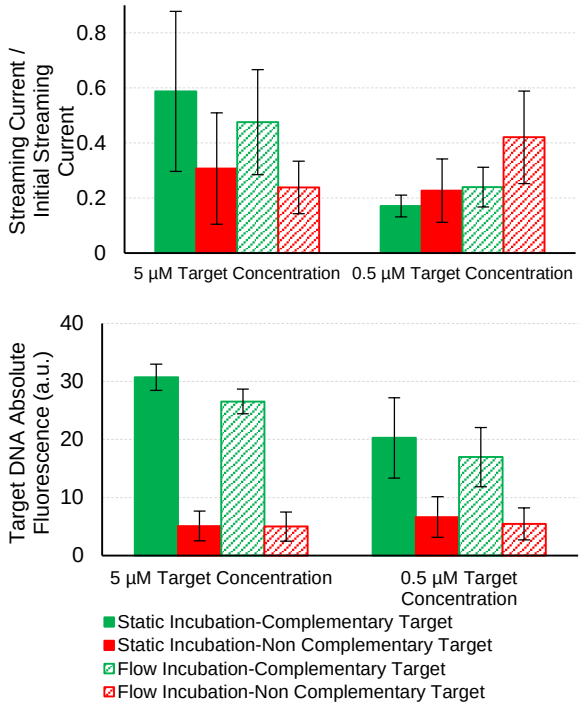

Figure 7 – Streaming current (top) and target fluorescence (bottom) after static or flow incubation of target DNA. Readings performed with 10mM PB. The error bars represent the standard deviation due to inter-experimental and device batch variations.

The results above indicate that the target steady-state incubation and flow incubation techniques performed yield comparable results in terms of both streaming current and fluorescence. This was not expected, as a continuous flow of target molecules should contribute to saturate the immobilized probe. However, the flow conditions were not completely optimized and were based on the incubation conditions used by (Silva, 2013). At a flow rate of 0.5 µl/min, the solution inside the channel was refreshed 31 times per minute. This refreshing rate should be optimized so that the shear stress doesn't hinder the target molecules from being recognized by the probes and settling on the surface.

4.3.3. DNA Surface Density Determination Using Fluorescence

In order to better describe the surface and confirm the previous estimates of the surface coverage by the ssDNA probe (coverage of about 19% after the immobilization, dropping to about 9% after the BSA blocking step), a spotting experiment was performed.

To calculate the DNA densities, typical dimensions of ssDNA were considered: 1 nm of width and 0.34 nm of length for each nucleotide. (Berg, et al., 2007) Given that the probe (and the target) has 22 nt, its length is about 7.48 nm. The area of a ssDNA probe immobilized with the phosphate backbone against the APTES surface should occupy a surface of about 7.48×10^{-6} µm^2. Thus, the surface density of a monolayer of ssDNA is around $\sigma = 1.337 \times 10^5$ µm^{-2} = 1.337×10^{13} cm^{-2}.

For the densities around the expected monolayer density, it was possible to make a power regression (fits better to the data than a linear regression) in order to obtain an expression to calculate the density of probe DNA molecules (σ) from the absolute probe fluorescence value (I):

$$\sigma = \left(\frac{I}{5.68 \times 10^{-5}}\right)^{\frac{1}{1.29}} \quad (16)$$

This expression was used to calculate the probe density in the experiment that detected 5 µM target DNA by incubation. After the probe immobilization, its surface density is 2.09×10^4 µm^{-2}, corresponding to 15.7% of the monolayer and, after the blocking step, drops to about 9.71×10^3 µm^{-2}, which is 7.3% of the expected monolayer density.

5. Conclusions

The recent discovery of circulating miRNAs has opened the possibility to study this class of biologically active agents as biomarkers of disease. From the state-of-the-art techniques for miRNA profiling reviewed on this thesis (NB, microarrays, qRT-PCR, and NGS), qRT-PCR is probably the most suited for circulating miRNA profiling, given the analyte's scarse concentrations in the body fluids (fM). Despite their availability, these laboratory techniques are laborious, expensive and time demanding.

LOC systems may play a decisive role in the POC profiling of miRNAs for diagnostic purposes. µTAS are able to integrate multiple functional elements into a single compact device, such as pumping, flow control, filtering, separation, concentration and detection. In this thesis, an electrical label-free detection principle was explored. Transient streaming current measurements in microfluidic channels (16 nL) were used for the detection of DNA hybridization. Fluorophore-labelled DNA probe and target molecules were employed in order to use fluorescence imaging to prove the streaming current measurements.

The transient streaming current and potential measurements proved to be accurate and robust in describing the overall surface charge of the channel. Using a bare channel in contact with different saline solutions, ζ-potentials were calculated using the streaming current and the streaming potential, yielding similar results, which are comparable to values in the literature. ζ-potential values varied between -67 mV for DI Water and - 4.6 mV for 100 mM PB. The dependencies of the ζ-potential and the conductivity on the ionic concentration were discussed and compared to the literature, proving the validity of the electrokinetic measurements on the microchannel.

In order to perform the capture and recognition of

the target DNA, the microchannel surface was functionalized with APTES to confer it with a positive charge. Afterwards, the negatively charged ssDNA probe was electrostatically immobilized to the APTES and the surface blocked to minimize non-specific adsorption of target molecules directly to the surface. The streaming current and fluorescence were measured, step by step, allowing to explain the evolution of the surface charge and probe coverage.

The system developed and characterized was able to distinguish between a ssDNA complementary target (miR-122 sequence) and a non-complementary control (miR-375) using both electrokinetic and optical detection methods. The streaming current measurements allowed to detect 5 µM of target DNA while the fluorescence measurements detected down to 500 nM target DNA.

The optimal PB concentration for the transient streaming current readings was 10 mM, yielding the best complementary/non-complementary signal ratio. BSA proved to be a better blocking agent when compared to salmon sperm DNA and to a control (no blocking). Steady state incubation and flow incubation of the target DNA molecules was compared, yielding similar results. However, the flow rate and duration of the incubation was not fully optimized.

The microchannel functionalization protocol proved not to be reproducible enough for low-deviation streaming current measurements for biomolecule detection. The streaming current is sensitive to the overall charge near the surface (in a thickness of the order of the Debye length), and its measurement represents the average charge on the surface, that is due to the APTES, the ssDNA probe, BSA and the target DNA. It was proved that the density of probe molecules on the surface is relatively low. After the probe immobilization, the estimated density of molecules is 2.09x104 µm-2, corresponding to 15.7% of a dense monolayer and, after the blocking step, it dropped to about 9.71x103 µm-2, which is 7.3% of the expected monolayer density. Having these values in mind, it is safe to say that the specific target hybridization represents less than 10% of the overall channel charge, and hence, of the streaming current measurement after target hybridization. Given the errors associated to the measurements, the target hybridization contribution is marginal, which explains the large error bars associated to the streaming current measurements and the trouble in distinguishing a complementary from a non-complementary target. In this protocol, the fluorescence is obviously more specific than the streaming current because only the fluorophore-labelled DNA molecules contribute actively to the optical measurements.

A robust surface functionalization protocol should be developed in the future. Different buffers, with low salt effects, should be tested. Alternated flow instead of pulsed flow should be used. Electrokinetic pumps could be integrated in the microfluidic system, allowing the autonomous, non-mechanical pumping of solutions. It should be assessed whether the adsorption of molecules onto the electrodes affects the measurements or not. Also, a temperature control system should be integrated with the microfluidic device.

6. References

Baldwin, R. L., 1996. How Hofmeister ion interactions affect protein stability. *Biophys J, 71(4),* p. 2056–2063.

Bard, A. J. & Faulkner, L. R., 2001. *Electrochemical Methods-Fundamentals and Applications.* 2nd. ed. New York: John Wiley & Sons, Inc.

Bartel, D. P., 2004. MicroRNAs: Genomics, Biogenesis, Mechanism, and Function. *Cell,* 116, p. 281–297.

Benes, V. & Castoldi, M., 2010. Expression profiling of microRNA using real-time quantitative PCR, how to use it and what is available. *Methods, 50(4),* p. 244-9.

Berg, J. M., Tymoczko, J. L. & Stryer, L., 2007. *Biochemistry.* 6th ed. New York: W. H. Freeman and Company.

Bruus, H., 2008. *Theoretical Microfluidics.* USA: Oxford University Press.

Chen, Y., Gelfond, J. A., McManus, L. M. & Shireman, P. K., 2009. Reproducibility of quantitative RT-PCR array in miRNA expression profiling and comparison with microarray analysis. *BMC Genomics, 10,* p. 407.

Fernández, D. P., Mulev, Y., Goodwin, A. R. H. & Sengers, J. M. H. L., 1995. A Database for the Static Dielectric Constant of Water and Steam. *J. Phys. Chem. Ref. Data, 24(33).*

Ge, S., Kojio, K., Takahara, A. & Kajiyama, T., 1998. Bovine serum albumin adsorption onto immobilized organotrichlorosilane surface: influence of the phase separation on protein adsorption patterns. *J Biomater Sci Polym Ed, 9(2),* p. 131-50.

Git, A. et al., 2010. Systematic comparison of microarray profiling, real-time PCR, and next-generation sequencing technologies for measuring differential microRNA expression. *RNA, 16(5),* p. 991-1006.

Grier, S. H. B. &. D. G., 2001. The Charge of Glass and Silica Surfaces. *J. Chem. Phys. 115,* p. 6716-6721.

Gubala, V. et al., 2013. Simple approach to study biomolecule adsorption in polymeric microfluidic channels. *Anal Chim Acta, 760,* p. 75-82.

Kinet, V., Halkein, J., Dirkx, E. & DeWindt, L. J., 2013. Cardiovascular extracellular microRNAs: emerging diagnostic markers and mechanisms of cell-to-cell RNA communication. *Frontiers in Genetics,* 4, p. 214.

Kirby, B. J. & Hasselbrink, E. F., 2004. Zeta potential of microfluidic substrates: 1. Theory, experimental techniques, and effects on separations. *Electrophoresis 25,* p. 187–202.

Kirby, B. J. & Hasselbrink, E. F., 2004. Zeta potential of microfluidic substrates: 2. Data for polymers. *Electrophoresis, 25,* p. 203–213.

Kong, W., Zhao, J.-J., He, L. & Cheng, J. Q., 2009. Strategies for profiling microRNA expression. *J Cell Physiol, 218(1),* p. 22-5.

Koshiol, J. et al., 2010. Strengths and Limitations of Laboratory Procedures for MicroRNA Detection. *Cancer Epidemiol Biomarkers Prev, 19(4),* p. 907-11.

Lameiras, F. S. et al., 2008. Measurement of the zeta potential of planar surfaces with a rotating disk. *Mat. Res, 11(2).*

Liu, C.-G., Spizzo, R., Calin, G. A. & Croce, C. M., 2008. Expression profiling of microRNA using oligo DNA arrays. *Methods, 44(1),* p. 22-30.

Martins, D. C., Chu, V., Prazeres, D. M. F. & Conde, J. P., 2011. Electrical detection of DNA immobilization and hybridization by streaming current measurements in microchannels. *Appl. Phys. Lett., 99,* p. 183702.

Martins, D. C., Chu, V., Prazeres, D. M. F. & Conde, J. P., 2013. Streaming currents in microfluidics with integrated polarizable electrodes. *Microfluid Nanofluid, 15,* p. 361–376.

Mohr, P. J., Taylor, B. N. & Newel, D. B., 2012. CODATA Recommended Values of the Fundamental Physical Constants: 2010. *Rev. Mod. Phys, 84, 1527.*

Moltzahn, F. et al., 2011. High throughput microRNA profiling: optimized multiplex qRT-PCR at nanoliter scale on the fluidigm dynamic arrayTM IFCs. *J Vis Exp, (54),* p. 2552.

Schmittgen, T. D., Jiang, J., Liu, Q. & Yang, L., 2004. A high-throughput method to monitor the expression of microRNA precursors. *Nucleic Acids Res, 32(4),* e43.

Silva, M., 2013. Detection of circulating miRNAs using microfluidics – a diagnostic method for cardiovascular diseases.Biotechnology M.Sc. Thesis. *IST, Portugal.*

Sze, A., Erickson, D., Ren, L. & Li, D., 2003. Zeta-potential measurement using the Smoluchowski equation and the slope of the current–time relationship in electroosmotic flow. *Journal of Colloid and Interface Science 261,* p. 402–410.

Tang, F. et al., 2006. 220-plex microRNA expression profile of a single cell. *Nat Protoc, 1(3),* p. 1154-9.